Energy Spectra of Neutrons Emitted Following π^- Capture in C, Al, Cd, Pb, and U†

H. L. ANDERSON, E. P. HINCKS,* C. S. JOHNSON,‡ C. REY, AND A. M. SEGAR§
The Enrico Fermi Institute for Nuclear Studies, The University of Chicago, Chicago, Illinois
(Received 21 August 1963)

The neutron emission from the capture of stopped π^- mesons in C, Al, Cd, Pb, and U has been studied using a time-of-flight detector. The energy spectra are characterized by a low-energy "evaporation" part, and a high-energy component due to the "direct" neutron emission. The general features of the "direct" neutron emission are similar for all the substances studied, with approximately 2 neutrons per π^- capture. In contrast, the relative yield of the low-energy component increases markedly in the heavier nuclei. The neutron multiplicities in the energy range from about 1.8 to 150 MeV were 2.8 ± 0.3, 3.2 ± 0.3, 3.6 ± 0.4, 3.5 ± 0.4, and 5.0 ± 0.5, for C, Al, Cd, Pb, and U, respectively. The total kinetic energy in neutron emission was about 68, 74, 80, 69, and 100 MeV for C, Al, Cd, Pb, and U, respectively. In the case of Cd the data are sufficiently complete to give a good account of the energy balance.

I. INTRODUCTION

THE capture of a slow π^- meson by a complex nucleus is seen most vividly in photographic emulsion where the process can give rise to a star. The absorption of the pion results in the release of about 140 MeV and this energy must be disposed of in some way. Studies of the process using emulsion,[1,2] the cloud chamber,[3] and the bubble chamber[4] have centered around the charged particles which make the star visible. It is clear, however, that the charged particles can account for only a small fraction of the available energy. The dominant process must be neutron emission, which is not restrained by the Coulomb barrier of the residual nucleus. In fact, the emulsion studies[1,2] have shown that in one third of the π^- captures in emulsion no visible charged particle tracks at all are seen. Yet there has been little direct experimental information about the neutron emission. Tongiorgi and Edwards[5] obtained the neutron yields from a number of elements by comparing the slow neutron density in a paraffin geometry with that produced by a calibrated RaαBe source. An important experiment by Ozaki *et al.*[6] showed that high-energy nucleons are emitted, with correlation at 180°, and that, at least in carbon, the emission of such correlated neutron-neutron pairs is about 5 times more frequent than the emission of neutron-proton pairs. This is evidence that the primary capture process is mediated mainly by a neutron-proton pair in the nucleus. The energy spectrum of neutrons from stopped π^- in emulsion has recently been reported by Barkow *et al.*[7] Besides these three experiments we are aware of no other published work in which the neutron emission from π^- capture in complex nuclei has been measured directly.[8]

In the present work we attempted to supply by rather simple measurements some of the missing information in the π^- capture reaction. We were able to obtain the number of neutrons as well as their energy distribution for elements of widely differing Z and A over the energy range from about 2 to 150 MeV. The energy was determined by time-of-flight. This method gives a reliable measure of the energy but suffers from a rapid deterioration in resolution as the energy increases. The derivation of the absolute yields depends on a calculation of the detection efficiency based on a knowledge of the cross sections and other factors. This limits the accuracy; it was, however, judged adequate in the present circumstances.

II. ARRANGEMENT

The 150-MeV/c negative meson beam produced by the University of Chicago synchrocyclotron was used in this experiment. After the beam emerged from the cyclotron fringing field it traversed the 12-ft-thick steel shield through a 6-in.-diam vacuum pipe. Upon entering the experimental area through the vacuum pipe the

† Research supported by the Office of Naval Research.
* Present address: Division of Pure Physics, National Research Council of Canada, Ottawa, Ontario, Canada.
‡ Present address: Naval Ordnance Test Station, China Lake, California.
§ Present address: Rutherford High Energy Laboratory, Chilton, Didcot, England.

[1] M. Demeur, A. Huleux, and G. Vanderhaeghe, Nuovo Cimento 4, 509 (1956). This paper contains references to earlier work. See also G. Vanderhaeghe and M. Demeur, Nuovo Cimento 4, Suppl. 2, 931 (1956).

[2] N. A. Perfilov, O. V. Lozhkin, and V. P. Shamov, Zh. Eksperim. i Teor. Fiz. **28**, 655 (1955) [translation: Soviet Phys.—JETP **1**, 439 (1955)]; A. A. Varfolomeev and R. I. Gerasimova, Zh. Eksperim. i Teor. Fiz. **30**, 1166 (1956) [translation: Soviet Phys.—JETP **3**, 988 (1957)]; S. A. Azimov, U. G. Guliamov, E. A. Zamchalova, M. Nizametdinova, M. I. Podgoretskii, and A. Iuldashev, Zh. Eksperim. i Teor. Fiz. **31**, 756 (1956) [translation: Soviet Phys.—JETP **4**, 632 (1957)]; G. Brown and I. S. Hughes, Phil. Mag. **2**, 777 (1957); A. T. Varfolomeev, Zh. Eksperim. i Teor. Fiz. **35**, 540 (1958) [translation: Soviet Phys.—JETP **8**, 373 (1959)]; A. Alumkel, A. G. Barkow, G. Kane, R. E. McDaniel and Z. O'Friel, Nuovo Cimento **17**, 316 (1960); N. B. Rabin, A. O. Weissenberg, and E. D. Kolganova, Phys. Letters **2**, 110 (1962).

[3] P. Ammiraju and L. M. Lederman, Nuovo Cimento 4, 283 (1956).

[4] M. Schiff, R. H. Hildebrand, and C. Giese, Phys. Rev. **122**, 265 (1961).

[5] V. C. Tongiorgi and D. A. Edwards, Phys. Rev. **88**, 145 (1952).

[6] S. Ozaki, R. Weinstein, G. Glass, E. Loh, L. Neimala, and A. Wattenberg, Phys. Rev. Letters **4**, 533 (1960).

[7] A. G. Barkow, C. E. Edmund, F. E. Penaranda, G. Kane, and Z. O'Friel, Nuovo Cimento **28**, 673 (1963).

[8] Some measurements of the neutron energy spectra from π^- capture by several elements have recently been made at Berkeley. S. N. Kaplan (private communication).

beam was deflected through 60° by a steering magnet into the counter telescope. A differential range curve of the beam taken with $\frac{1}{16}$-in. Cu in the target position is shown in Fig. 1.

The counter arrangement is shown in Fig. 2. Counters 1 through 5 were square plastic scintillators attached to Lucite light pipes through which they were viewed by RCA-6810A photomultipliers. Counter C was a water Čerenkov counter used to reject electrons in the beam. The neutron detector consisted of liquid scintillator (type NE 213)[9] contained in a cylindrical Lucite box whose inside diameter and thickness were 3.75 and 1.25 in., respectively. The thickness of the wall facing the target was $\frac{1}{16}$ in. and that of the opposite wall which was in contact with the photomultiplier was $\frac{1}{8}$ in. The thickness of the side wall was $\frac{1}{4}$ in. The scintillator box was inside a thin-walled ($\frac{1}{16}$ in.) steel box which contained an aluminum oxide powder reflector and the assembly was attached to the face of an RCA-7046 photomultiplier. A neutron shield was provided consisting of sheet cadmium $\frac{1}{16}$ in. thick (not shown in Fig. 2), surrounded by a mixture (equal parts by weight) of paraffin and lithium carbonate. Background from gamma rays was greatly reduced by using the scintillator decay time discriminator method, described below, to reject electrons.

The thicknesses of the C, Al, Cd, Pb, and U targets were 2.03, 5.35, 5.54, 5.78, and 5.48 g/cm², respectively. They were all rectangular with dimensions 4 in. by 6 in. and were positioned at 45° to the incident beam. For a maximum pion stopping rate the absorber shown in Fig. 2 was omitted with all targets except carbon. For the C target, which was thinner than the other targets, a $\frac{1}{4}$-in. Al absorber was required.

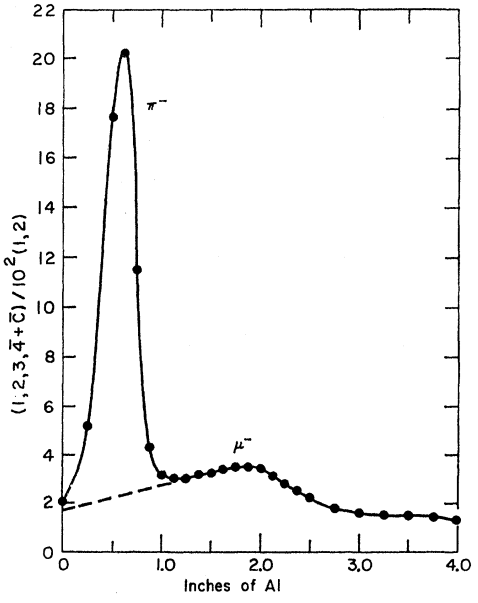

FIG. 1. Differential range curve of the negative 150-MeV/c meson beam. The ordinate gives the relative number of pions and muons stopping in a $\frac{1}{16}$-in. Cu target.

[9] Available from Nuclear Enterprises Ltd., Winnipeg, Canada.

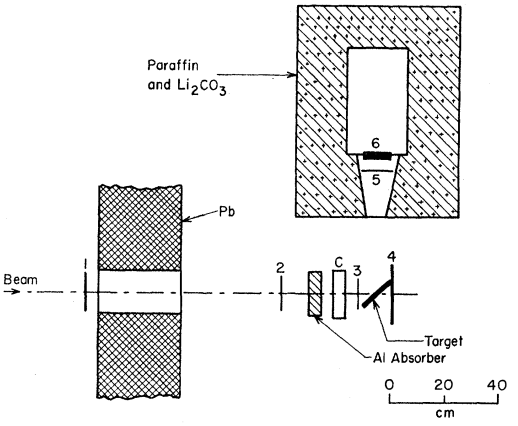

FIG. 2. Top view of the experimental arrangement. Counters 1, 2, 3, 4, and 5 are plastic scintillators. C is a water Čerenkov counter.

III. ELECTRONICS

A block diagram of the electronics is shown in Fig. 3. Pulses from the telescope counters and counter 5 were amplified by transistor limiting amplifiers and clipped to about 2×10^{-8}-sec width before being fed into the coincidence-anticoincidence circuit. A stopping π^- produces a $(1,2,3,\bar{4}+\bar{C})$ event, where the bar means anticoincidence. A $(1,2,3,\bar{4}+\bar{C})$ event produces pulses about 10^{-7} sec long at both coincidence circuit A and anticoincidence circuit B. Pulses from counters 1 and 5 are also fed into A. If there is a pulse from 1 or 5 in coincidence with the $(1,2,3,\bar{4}+\bar{C})$ pulse at A, an output pulse is fed into the anticoincidence circuit B and prevents the $(1,2,3,\bar{4}+\bar{C})$ pulse from initiating a "prime pulse" for the time-to-pulse-height converter (TPHC). The delays are adjusted so that only pulses from 1 following the initial stopping π^- pulse can be in coincidence at A. This is to ensure that the neutron de-

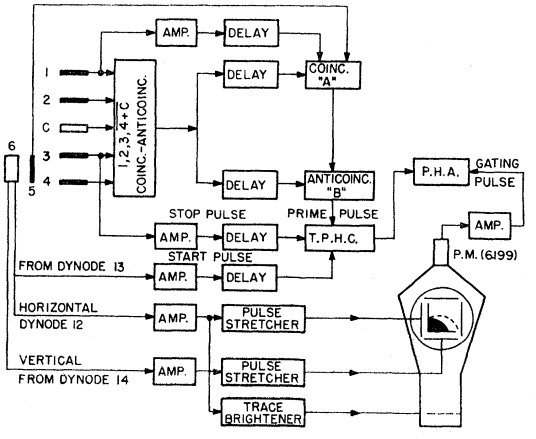

FIG. 3. Block diagram of the electronics. TPHC is the time-to-pulse-height converter and PHA is the pulse-height analyzer.

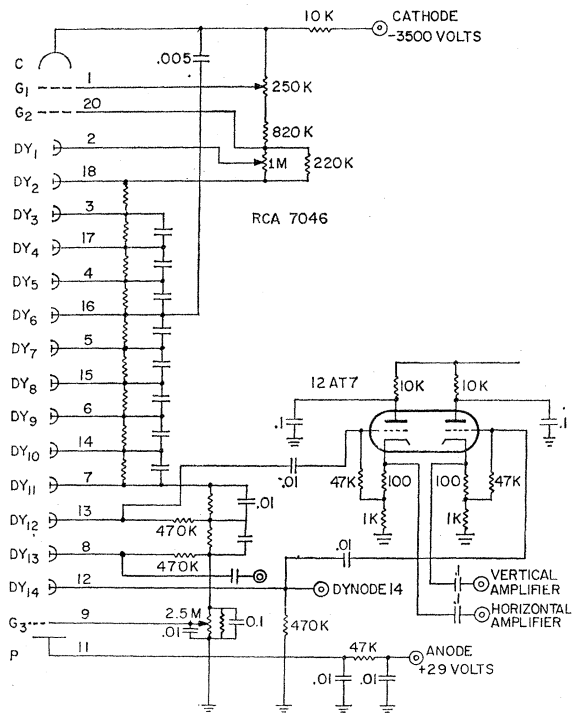

FIG. 4. Circuit used with RCA-7046 phototube for decay time discrimination between neutrons and gamma rays. Unspecified resistors and capacitors are 100 K and 0.001 μF, respectively.

tected by 6 is due to the pion which produced the $(1,2,3,\bar{4}+\bar{C})$ event and not due to a later one. If there is no anticoincidence pulse at B the $(1,2,3,\bar{4}+\bar{C})$ pulse activates the TPHC with a 225-nsec-long prime pulse. The TPHC with its associated pulse-height analyzer (PHA) is then ready to measure the time difference between a pair of pulses, one of which comes from counter 3 and one from counter 6. A pulse from counter 6 occurring during the prime pulse produces a "start" pulse at the TPHC. The pulse produced in 3 by the stopping π^- is delayed and provides the "stop" pulse. If the 3 and 6 pulses were not inverted in time as indicated, that is if their roles of start and stop pulses were interchanged, the PHA dead time would be excessive because the PHA would be required to analyze all $(1,2,3,\bar{4}+\bar{C},\bar{1}+\bar{5})$ events regardless of whether or not there was a pulse from 6. The TPHC used here is the Culligan and Lipman design.[10] The other circuits used were developed in this laboratory and are described in detail elsewhere.[11]

Gamma rays and neutrons detected by counter 6 were distinguished by the method of pulse-shape discrimination first suggested by Brooks.[12] This method depends on the fact that for certain scintillators the slow components of the scintillation light from a proton recoil contain relatively more energy than they do in the case of a less densely ionizing electron.

The shape discrimination circuit used here is based on the photomultiplier saturation technique which was introduced by Owen.[13] If the potential difference between the last dynode of the photomultiplier (dynode No. 14 in our case) and the anode is made small, space-charge limitation of the anode current produces a strong nonlinearity of the photomultiplier current gain as measured at dynode 14. [If β is the secondary emission multiplication factor of dynode 14, the photomultiplier current gain can obviously vary from its normal no-saturation value a_0 to $a_0/(\beta-1)$, depending both on the current into the dynode and on the dynode-anode potential.] In the usual application of Owen's technique the anode voltage is adjusted so that the large amplitude fast component of the signal produces a net negative current, and the small amplitude slow component produces a net positive current into the last dynode. After integration the resultant voltage pulse V' may be negative for neutrons and positive for gamma rays. The main advantages of this circuit are its simplicity and ease of adjustment, but the discrimination between gamma rays and neutrons by the polarity of V' can only be realized over a restricted region of pulse amplitudes for a given anode voltage setting. To avoid this limitation we used a cathode-ray oscilloscope (CRO) display in which each event in the scintillator appeared as a dot whose vertical displacement depended on V' and whose horizontal displacement depended on V, the integrated pulse without saturation which was obtained from dynode 12.

A block diagram of the discriminator is given in

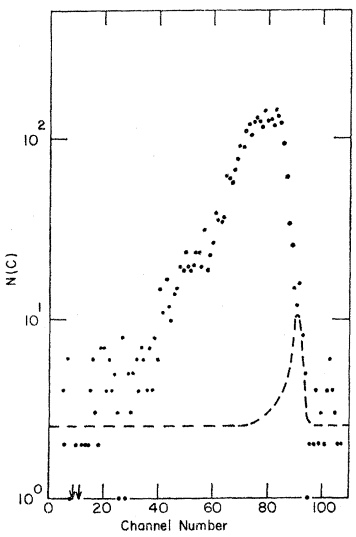

FIG. 5. Time-of-flight spectrum of neutrons from π^- captures on carbon. Dashed curve indicates random background and prompt gamma rays.

[10] G. Culligan and N. H. Lipman, Rev. Sci. Instr. **31**, 1209 (1960).

[11] R. Gabriel and A. M. Segar, Nucl. Instr. & Methods **12**, 307 (1961).

[12] F. D. Brooks in *Progress in Nuclear Physics* edited by O. R. Frisch (Pergamon Press, Inc., London, 1956), Vol. 5, p. 284; Nucl. Instr. Methods **4**, 151 (1959).

[13] R. B. Owen in *Nuclear Electronics* (International Atomic Energy Agency, Vienna, 1959), Vol. 1, p. 27; Nucleonics **17**, 92 (1959).

Fig. 3 while Fig. 4 shows the details of the RCA-7046 photomultiplier circuit. The integrated pulses from dynodes 12 and 14 were amplified by slow amplifiers and then stretched by circuits similar to those designed by Bernstein *et al.*[14] To increase the dynamic range of the discriminator the amplifiers were made highly nonlinear; positive and negative pulses from dynode 14 were separately stretched in parallel circuits. The stretched outputs were applied to the CRO horizontal and vertical deflection plates, and a delayed pulse derived from V was used to intensify the CRO beam for about one microsecond after the deflecting voltages had reached full amplitude. The dots produced by neutrons and gamma rays appear separately clustered about two different loci corresponding to their different values of V' for any given V. The CRO which has a fast phosphor (P-15, decay time 1.7 μsec) was viewed by a one-inch photomultiplier and the unwanted events were removed by a mask. The output pulses from the one-inch photomultiplier (Type 6199, operated at about 500 V) were used to gate the PHA.

No difficulty was experienced in obtaining uniform output pulses regardless of the position of the dot on the CRO screen. The 7046 photomultiplier anode voltage was adjusted for optimum separation of neutrons and gamma rays at low energies. Below the pulse height corresponding to a proton of about one MeV, the neutron and gamma-ray distributions began to merge, and so when neutrons were selected, a gamma-ray contamination was included. Above this point the distributions were well resolved and an efficiency of essentially 100% for recording neutrons was achieved with no significant gamma-ray contamination. The nonlinearity of the horizontal and vertical amplifiers ensured that the neutron pattern remained within the aperture set by the mask, and resolved from the gamma-ray pattern, for the largest pulses expected. To aid in the adjustment and to provide a visual monitor of the behavior of the discriminator a second CRO, identical to the first but with a P-2 phosphor, was operated in parallel with it. All adjustments were made using a Po-Be neutron (and gamma-ray) source, a Co^{60} gamma-ray source, and the room background with the π^- beam on. Unfortunately, quantitative measurements were not made of the loss of efficiency at low energies.

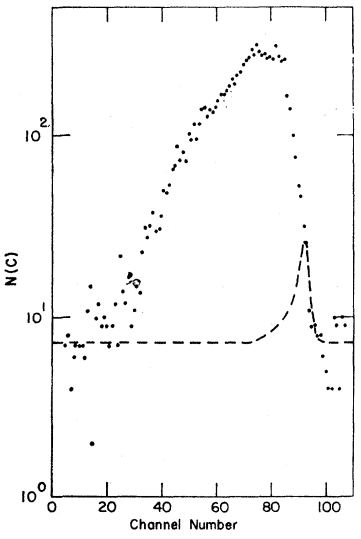

FIG. 6. Time-of-flight spectrum of neutrons from π^- captures on aluminum. Dashed curve indicates random background and prompt gamma rays.

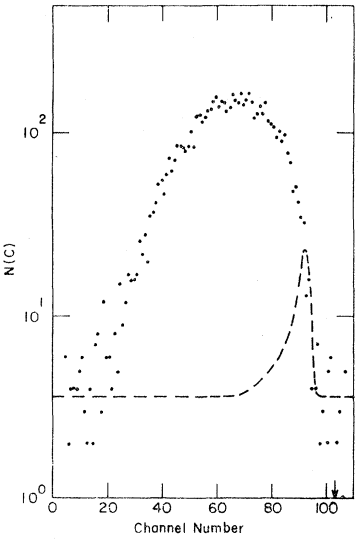

FIG. 7. Time-of-flight spectrum of neutrons from π^- captures on cadmium. Dashed curve indicates random background and prompt gamma rays.

IV. MEASUREMENTS

All the neutron time-of-flight spectra were taken with the same flight path (108.3 cm). Each target was run several times, the targets being changed at the end of one-hour runs. The accumulated spectra from these individual runs are shown plotted in Figs. 5 through 9. Also shown in each of these figures is the random background plus the estimated intensity of prompt gamma rays not rejected by the neutron-gamma discriminator. Time zero (for the time-of-flight spectra) was determined by running with the uranium target for 15 min $[1.76\times10^6$ $(1, 2, 3, \bar{4}+\bar{C})$ counts] at a flight path of 56.2 cm and selecting gamma-ray events in counter 6. This gamma-ray time-of-flight spectrum is shown in Fig. 10. Time zero was calculated as the mean peak position of the prompt gamma-ray spectrum after subtracting the tail of the distribution. After correcting for the difference in flight path used for the neutron and gamma measurements, and taking into account the finite flight time of gamma rays, time zero was found to be at channel 96.1±0.5. The time scale was calibrated using counter 3 to provide the prime pulse as well as the stop pulse to the TPHC. A series of coincidence peaks was obtained by placing a Co^{60} source near 3 and varying the delay of 6 by known amounts. Making a three parameter polynomial least-squares fit to the delay versus coincidence peak position data we obtained the

[14] W. Bernstein, R. L. Chase, and A. W. Schardt, Rev. Sci. Instr. 24, 437 (1953).

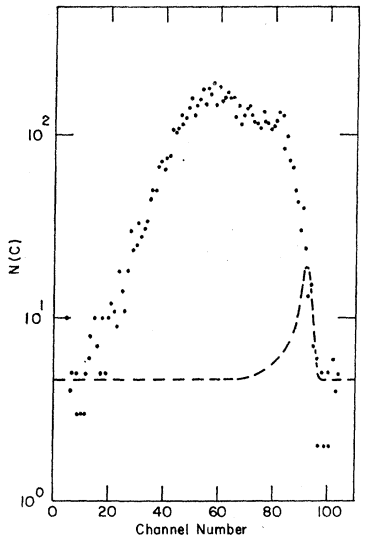

FIG. 8. Time-of-flight spectrum of neutrons from π^- captures on lead. Dashed curve indicates random background and prompt gamma rays.

following relation between time (t) in nanoseconds, and PHA channel (C):

$$t=118.0-1.297C+7.195\times10^{-4}C^2 \text{ nsec.} \quad (1)$$

V. DATA REDUCTION

Reduction of the data consisted mainly of converting the neutron time-of-flight spectra to energy spectra, and making the efficiency and solid-angle corrections to these spectra. Conversion of the time distributions obtained from the PHA to the energy spectra $[N(E)]$ was done using the formula:

$$N(E)=\frac{N(C)-G(C)-B}{MF\Omega\epsilon(E)\Delta E(C)}, \quad (2)$$

where $N(C)$ is the number of counts and $G(C)$ is the number of prompt gamma rays in channel C. B is the constant random background per channel, F is the fraction of $(1,2,3,\bar{4}+\bar{C})$ counts (M) due to π^- stopping in the target, Ω is the fractional solid angle, $\epsilon(E)$ is the calculated counter efficiency and $\Delta E(C)$ is the width of channel C in MeV. E is the kinetic energy calculated from the known flight path and Eq. (1), taking into account relativistic effects. The data plotted in Figs. 5 through 9 are presented in Table I. At the low-energy end of the spectra several channels have been combined because of the smallness of the energy intervals corresponding to these channels. Columns one, two, and three of Table I give the channels and related time and energy intervals. In column four are listed the central energies of the intervals. The random background per channel for each interval is given below Table I.

A. Random Background and Prompt Gamma Rays

The magnitude of the background per channel B was assumed to be constant over the time spectrum. It was calculated from that portion of the spectrum in the channels (95 through 104) above time zero, (i.e., negative flight times) and from those channels (5 through 12) below the minimum energy channel. The minimum energy was taken as the channel in which the intensity of the extrapolated uranium time distribution reached the level of the random background intensity (channel 12.5 or 0.59 MeV).

As mentioned in Sec. III the neutron-gamma discriminator did not eliminate all the low-energy gamma rays and it was necessary to subtract the prompt gamma rays not rejected. Gamma rays occurring randomly in time and not rejected by the discriminator are included in the subtraction of the random background. The shape of the prompt gamma-ray spectrum was assumed to be that given in Fig. 10 and the intensity was estimated by equating the prompt spectrum counts to the neutron spectrum counts in channels 92 through 100. Few true neutrons are expected in this region because of the rapid decline of the prompt peak on the high-energy side which is an indication of counter resolution. The spectrum of prompt gamma rays plus random background which is to be subtracted in each case is indicated by the dashed curves in Figs. 5 through 9.

B. Neutron Counter Efficiency

The neutron counting efficiency of plastic scintillators over the range of energy between 0 and 10 MeV has been studied in considerable detail[15–17] and its computation is a straightforward problem. However, for energies above 10 MeV, the cross section for inelastic scattering

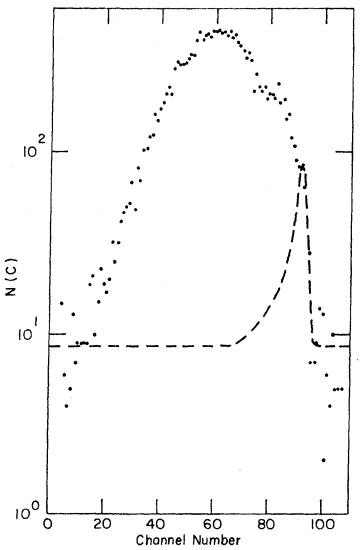

FIG. 9. Time-of-flight spectrum of neutrons from π^- captures on uranium. Dashed curve indicates random background and prompt gamma rays.

[15] C. D. Swartz and G. E. Owen in *Fast Neutron Physics*, edited by J. B. Marion and J. L. Fowler (Interscience Publishers, Inc., New York, 1960), Part I, p. 221.
[16] J. E. Hardy, Rev. Sci. Instr. **29**, 705 (1958).
[17] R. Batchelor, W. B. Gilboy, J. B. Parker, and J. H. Towle, Nucl. Instr. Methods **13**, 70 (1961).

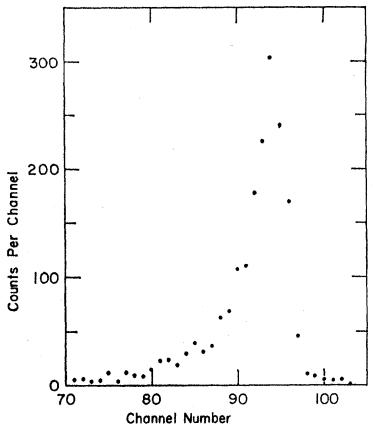

FIG. 10. Time-of-flight spectrum of gamma rays from π^- on uranium with the neutron-gamma-ray discriminator accepting only gamma rays.

on carbon is appreciable and its contribution to counter efficiency is difficult to estimate. Batchelor *et al.*[17] have made Monto Carlo calculations of counter efficiencies up to 14 MeV taking into account elastic and inelastic scattering from carbon. At energies above 14 MeV the cross sections for the dominant inelastic neutron-carbon reactions are not known in sufficient detail to justify detailed Monte Carlo calculations. We have therefore adopted the procedure described below for estimating the neutron counter efficiency.

Counter efficiency is assumed to depend on the following processes: single and multiple scattering on hydrogen, single inelastic scattering from carbon, and single elastic scattering followed by an inelastic scattering on carbon. Elastic scattering on carbon can be shown to be unimportant from the following kinematic considerations. Recoil carbon nuclei produce much weaker scintillations than protons of the same energy. It would take a carbon nucleus of about 8 MeV[17] to produce the same amount of light in the scintillator as a proton with our minimum detectable energy ($\sim$0.6 MeV). It requires a neutron of about 30 MeV to produce an 8-MeV carbon nucleus assuming a maximum transfer of energy. However, such large transfers of energy are very improbable. For example, a neutron of 150 MeV must be scattered through a laboratory angle of about 45° in order to produce an 8-MeV carbon recoil and the differential cross section for scattering at this angle is very small.[18]

The contribution to counter efficiency from scattering on hydrogen may be expressed very simply, neglecting edge and end effects, by the following equation[15]:

$$\epsilon_H(E)=[1-\exp(-n_H\sigma_H L)](1-E_b/E), \qquad (3)$$

where n_H is the number of hydrogen atoms per unit volume of scintillator, L is the thickness of the scintillator, and σ_H is the hydrogen cross section at energy $E>E_b$, where E_b is the threshold for detecting a proton recoil and the minimum neutron energy detectable. Equation (3) was derived neglecting the presence of carbon, multiple scattering, and the nonlinearity of scintillator light output with proton energy. Edge and end effects can be neglected because the range of a detectable proton in the scintillator is very small compared to its dimensions. Although these assumptions are an over-simplification, it turns out that the results of this formula agree very well, over the energy range from E_b to 10 MeV, with detailed Monte Carlo calculations[17] in which these other effects are taken into account.

To take into account the distribution in pulse heights obtained for a given proton recoil energy E_p we have to replace the term $(1-E_b/E)$ in Eq. (3) by

$$f=\frac{1}{E}\int_0^E dE_p\int_{E_b'}^{\infty} R(E_p'-E_p)dE_p', \qquad (4)$$

where E_b' is the energy corresponding to the bias at which the discriminator is set. We take

$$R(E_p'-E_p)=(2\pi\sigma^2)^{-1/2}\exp[-(E_p'-E_p)^2/2\sigma^2]. \qquad (5)$$

The value of σ was determined from a study of the pulse-height spectra of the 0.511- and 1.28-MeV gamma-ray lines in Na^{22}. The difference in pulse height for protons as compared with electrons of the same energy was corrected for and σ was taken to vary as $E^{1/2}$. For our case we took $\sigma=0.250$ and $E_b'=0.9\pm0.2$. We have no direct measure of E_b' but assume this value because it makes the efficiency very small at 0.60 MeV which is approximately our minimum detectable proton energy. The counter efficiency above 2 MeV is not very sensitive to the choice of E_b'. The

TABLE I. Time-of-flight data.

C (channels)	t (nsec)	E (MeV)	$\bar{E}$ (MeV)	$N(C)$[a] C	Al	Cd	Pb	U
48–52	58.6–52.5	1.78– 2.23	2.01	102	464	435	702	1616
53–56	52.5–47.6	2.23– 2.71	2.47	88	496	487	658	1695
57–59	47.6–44.0	2.71– 3.18	2.95	74	399	418	508	1327
60–61	44.0–41.6	3.18– 3.56	3.37	66	296	298	334	918
62–63	41.6–39.1	3.56– 4.02	3.79	71	337	298	330	895
64–65	39.1–36.7	4.02– 4.57	4.30	100	357	269	320	884
66	36.7–35.5	4.57– 4.88	4.73	61	205	162	125	423
67	35.5–34.3	4.88– 5.24	5.06	58	191	151	143	430
68	34.3–33.1	5.24– 5.63	5.44	68	215	149	114	396
69	33.1–31.9	5.63– 6.06	5.85	78	220	165	127	380
70	31.9–30.7	6.06– 6.55	6.31	92	245	143	139	361
71	30.7–29.5	6.55– 7.09	6.82	91	257	152	143	324
72	29.5–28.3	7.09– 7.71	7.40	110	265	165	129	345
73	28.3–27.2	7.71– 8.42	8.07	120	293	149	118	318
74	27.2–26.0	8.42– 9.22	8.82	106	278	121	116	216
75	26.0–24.8	9.22– 10.14	9.68	123	311	128	110	270
76	24.8–23.6	10.1 – 11.2	10.7	129	289	140	133	222
77	23.6–22.4	11.2 – 12.5	11.8	124	273	127	117	215
78	22.4–21.2	12.5 – 13.9	13.2	117	275	149	115	229
79	21.2–20.0	13.9 – 15.7	14.8	142	263	116	109	195
80	20.0–18.8	15.7 – 17.7	16.7	125	265	111	111	209
81	18.8–17.7	17.7 – 20.3	19.0	127	261	109	119	206
82	17.7–16.5	20.3 – 23.4	21.8	118	302	94	131	198
83	16.5–15.3	23.4 – 27.3	25.3	144	267	101	127	235
84	15.3–14.1	27.3 – 32.3	29.8	133	253	90	84	187
85	14.1–13.0	32.3 – 38.8	35.5	122	257	98	99	191
86	13.0–11.8	38.8 – 47.5	43.2	94	164	78	73	152
87	11.8–10.6	47.5 – 59.7	53.6	61	139	69	67	159
88	10.6– 9.4	59.7 – 77.4	68.6	34	99	48	50	120
89	9.4– 8.3	77.4 –105	91.2	26	76	51	43	108
90	8.3– 7.1	105 –152	128	15	52	42	30	90

[a] The backgrounds per channel for these targets were: 2.54 ± 0.34, 7.18 ± 0.57, 3.64 ± 0.41, 4.63 ± 0.49, and 8.73 ± 0.63 for carbon, aluminum, cadmium, lead, and uranium, respectively.

[18] C. J. Batty, Nucl. Phys. **23**, 562 (1961).

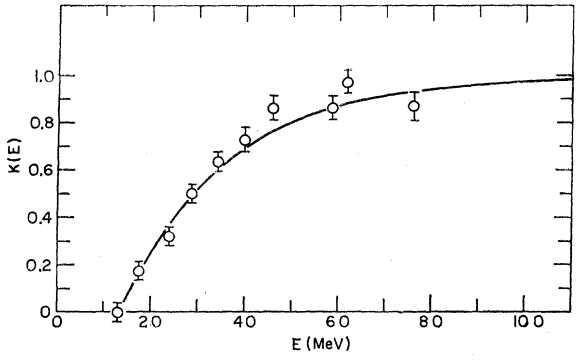

FIG. 11. Plot of the fraction of inelastic neutron scatterings on carbon which give a detectable light pulse versus energy.

data below 1.78 MeV were not used because of the large uncertainty in efficiency in this region.

To estimate the increase in efficiency due to inelastic scattering from carbon it is necessary to determine the fraction of scatterings that are detectable. This is done with the help of the experimental results of Wiegand *et al.*,[19] who have measured the neutron efficiency of a plastic scintillator over the range from 4 to 76 MeV. First we calculate the fraction of incident neutrons having an inelastic collision with a carbon nucleus. This is given by

$$\epsilon_1(E)=\frac{n_C\sigma_i(E)}{n_H\bar{\sigma}(E)}[1-\exp(-n_H\bar{\sigma}(E)L], \qquad (6)$$

where n_C and n_H are the numbers of carbon and hydrogen atoms per unit volume, respectively, $\sigma_i(E)$ is the inelastic carbon cross section at energy E, and $\bar{\sigma}(E)=\sigma_H(E)+(n_C/n_H)\sigma_t(E)$, where $\sigma_H(E)$ and $\sigma_t(E)$ are the total hydrogen and carbon cross sections at E. The fraction of neutrons having an elastic scattering on carbon within an element dx after a distance x in the scintillator, followed by an inelastic scattering within an element dy after distance y, when integrated over the path length l in the scintillator gives the following result,

$$\epsilon_2(E)=n_C^2\sigma_e(E)\sigma_i(E_1)\int_0^l \exp(-n_H\bar{\sigma}(E)x)dx \times\int_x^l \exp[-n_H\bar{\sigma}(E_1)(y-x)]dy. \qquad (7)$$

Here E_1 is the energy of the neutron after the first scattering and, following Swartz and Owen,[15] we assume for simplicity $E_1=0.85\ E$ and take l equal to the thickness (L) of the scintillator. For NE213 liquid scintillator $n_H=5.521\times10^{22}$, $n_C=4.455\times10^{22}$ atoms per cc. There are also 1.36×10^{19} atoms per cc of oxygen and an equal amount of nitrogen present, but these quantities are relatively small compared to the amounts of carbon and hydrogen and may be neglected. The total detection efficiency is now written as

$$\epsilon(E)=\epsilon_H(E)+K(E)[\epsilon_1(E)+\epsilon_2(E)], \qquad (8)$$

neglecting the small difference in energy between E_1 and E. Before we can calculate $\epsilon(E)$ from Eq. (8) we must find $K(E)$, the fraction of inelastic scatterings that are detectable. $K(E)$ is evaluated using the experimental results of Wiegand *et al.*,[19] who determined $\epsilon(E)$ experimentally. By computing $\epsilon_H(E)$, $\epsilon_1(E)$, $\epsilon_2(E)$ for their scintillator, we can solve Eq. (8) for $K(E)$. The results of these calculations are shown in Fig. 11. Assuming the data in Fig. 11 to have the form $K(E)=1-\exp[a(E-b)]$ we find by fitting the data

$$K(E)=1-\exp[-0.0440(E-13.27)], \qquad (9)$$

which is shown plotted with the data in Fig. 11. In evaluating $K(E)$ it has been assumed that the difference between our counter and that of Wiegand *et al.* (i.e.,

TABLE II. Data on number of stopping π^-.

Target	Total running time (hours)	M Total $(1,2,3,\bar{4}+\bar{C})$ counts (10^7)	F (Correction factor)
C	4	2.179	0.812
Al	7.5	5.216	0.748
Cd	4	2.467	0.790
Pb	4	2.568	0.803
U	7	4.215	0.806

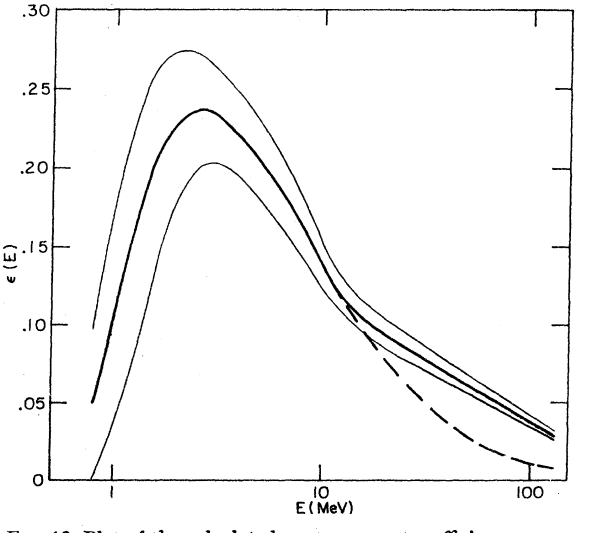

FIG. 12. Plot of the calculated neutron counter efficiency versus energy. The heavy line gives the efficiency; the two light lines indicate the estimated uncertainty in efficiency. The dashed curve gives the contribution to the efficiency from just the hydrogen in the scintillator.

[19] C. E. Wiegand, T. Elioff, W. B. Johnson, L. B. Auerbach, J. Lach, and T. Ypsilantis, Rev. Sci. Instr. **33**, 526 (1962). See also P. H. Bowen, G. C. Cox, G. B. Huxtable, A. Langsford, J. P. Scanlon, G. H. Stafford, and J. J. Thresher, Nucl. Instr. Methods **17**, 117 (1962).

TABLE III. Neutron energy spectra.[a]

	$N(E)\times10^2$				
$\bar{E}$	C	Al	Cd	Pb	U
2.01	10.3 ±2.4	21.9 ±4.7	43.5 ±9.3	67. ±14	94. ±20
2.47	8.0 ±1.6	21.8 ±3.5	44.2 ±7.0	56.5 ±8.8	89. ±14
2.95	7.1 ±1.3	18.2 ±2.7	39.3 ±5.7	45.0 ± 6.5	72. ±10
3.37	8.2 ±1.5	17.1 ±2.3	35.4 ±4.7	37.3 ± 4.9	62.8 ± 7.8
3.79	7.5 ±1.3	16.7 ±2.2	30.1 ±4.0	31.3 ± 4.1	52.0 ± 6.4
4.30	9.5 ±1.5	15.4 ±2.0	23.5 ±3.2	26.4 ± 3.5	44.7 ± 5.5
4.73	10.6 ±1.8	16.3 ±2.0	26.1 ±3.3	18.7 ± 2.6	39.1 ± 4.4
5.06	8.9 ±1.5	13.3 ±1.7	21.4 ±2.8	19.0 ± 2.5	35.1 ± 3.9
5.44	9.9 ±1.6	14.3 ±1.8	20.0 ±2.6	14.2 ± 2.0	30.6 ± 3.4
5.85	10.7 ±1.6	13.4 ±1.7	20.7 ±2.7	14.9 ± 2.0	27.4 ± 3.1
6.31	11.5 ±1.7	13.9 ±1.7	16.3 ±2.1	14.8 ± 2.0	23.6 ± 2.7
6.82	10.7 ±1.6	13.7 ±1.6	16.3 ±2.1	14.3 ± 1.9	19.8 ± 2.3
7.40	11.8 ±1.7	12.9 ±1.5	16.1 ±2.1	11.8 ± 1.6	19.3 ± 2.2
8.07	11.9 ±1.6	13.1 ±1.5	13.4 ±1.8	9.8 ± 1.4	16.3 ± 1.9
8.82	10.0 ±1.4	11.8 ±1.4	10.3 ±1.4	9.2 ± 1.3	10.4 ± 1.3
9.68	10.9 ±1.5	12.4 ±1.4	10.2 ±1.4	8.1 ± 1.2	12.3 ± 1.5
10.7	10.3 ±1.4	10.4 ±1.2	10.1 ±1.3	9.0 ± 1.2	9.0 ± 1.1
11.8	8.9 ±1.2	8.8 ±1.0	8.2 ±1.1	7.0 ± 1.0	7.9 ± 1.0
13.2	8.3 ±1.2	8.9 ±1.0	9.6 ±1.3	6.9 ± 1.0	8.4 ± 1.0
14.8	8.3 ±1.1	6.9 ±0.8	6.1 ±0.9	5.4 ± 0.8	5.8 ± 0.7
16.7	7.0 ±1.0	6.7 ±0.8	5.6 ±0.8	5.2 ± 0.7	6.0 ± 0.7
19.0	5.8 ±0.8	5.3 ±0.6	4.4 ±0.6	4.5 ± 0.6	4.8 ± 0.6
21.8	4.8 ±0.7	5.5 ±0.6	3.4 ±0.5	4.5 ± 0.6	4.1 ± 0.5
25.3	4.9 ±0.7	4.1 ±0.5	3.1 ±0.4	3.7 ± 0.5	4.1 ± 0.5
29.8	3.8 ±0.5	3.3 ±0.4	2.3 ±0.3	2.0 ± 0.3	2.7 ± 0.3
35.5	2.9 ±0.4	2.8 ±0.3	2.1 ±0.3	2.0 ± 0.3	2.3 ± 0.3
43.2	1.9 ±0.3	1.5 ±0.2	1.4 ±0.2	1.2 ± 0.2	1.5 ± 0.2
53.6	1.0 ±0.2	1.0 ±0.1	1.0 ±0.2	0.87± 0.14	1.3 ± 0.2
68.6	0.42±0.09	0.55±0.08	0.53±0.10	0.51± 0.10	0.76± 0.1
91.2	0.25±0.06	0.33±0.05	0.45±0.08	0.34± 0.07	0.54± 0.08
128.	0.11±0.03	0.17±0.03	0.30±0.06	0.19± 0.04	0.36± 0.06

[a] Uncertainties include uncertainty in counter efficiency.

differences in bias energy, size, composition, and discrimination) are not very important. Having obtained $K(E)$ it became possible to compute $\epsilon(E)$ for our counter from Eq. (8). The result of this calculation is given in Fig. 12.

C. Corrected $(1,2,3,\bar{4}+\bar{C})$ Counts

The total running time and $(1,2,3,\bar{4}+\bar{C})$ counts are given in columns two and three of Table II. Column four contains the estimated fraction (F) of $(1,2,3,\bar{4}+\bar{C})$ counts due to stopping pions. The quantity F is estimated from Fig. 1 in which the intensity of $(1,2,3,\bar{4}+\bar{C})$ counts not due to pions, i.e., due to electrons and muons, is indicated by the dashed line. The contribution to $(1,2,3,\bar{4}+\bar{C})$ due to pions which missed 4 due to scattering is small and was neglected here.

Applying Eq. (2) to the data in Table I we obtain the energy spectra given in Table III. The uncertainties given in Table III are calculated from the statistical uncertainties in the number of counts per channel, in the subtractions made, and from the uncertainty in the calculated neutron counter efficiency. The uncertainty in the calculated counter efficiency was assumed to be 10% due to uncertainties in cross section added in quadrature to the uncertainty from E_b'. No correction was applied for secondary neutrons which could be produced by $(n,2n)$ reactions in the target. Estimates showed that this correction was quite small compared to other uncertainties.

D. Resolution

The (time) resolution of the time-of-flight spectrometer was not measured directly, but can be estimated from the prompt gamma-ray peak (Fig. 10). The tail of the prompt peak is probably due to small pulses in the photomultiplier mainly from low-energy pi-mesonic x rays. A much smaller tail might be expected for the resolution function for the higher energy neutrons. We might expect therefore, that the time resolution for these neutrons is the width of the prompt gamma peak, after subtracting the tail, which is about 3 channels or 4 nsec (full width at half-maximum). Thus, at 10 MeV (25 nsec) the fractional energy resolution is $\Delta E/E=0.32$. At 100 MeV the energy resolution ($\Delta E/E=0.94$) is really quite poor. At the low end of the energy scale the resolution improves because t increases but now it would be proper to take into account the tail, which worsens the resolution. Because of the generally poor resolution we cannot expect our energy distribution to show any but the broadest features of the spectra.

VI. RESULTS

The general features of the neutron energy distributions exhibited in Table III and in Figs. 13–17 are

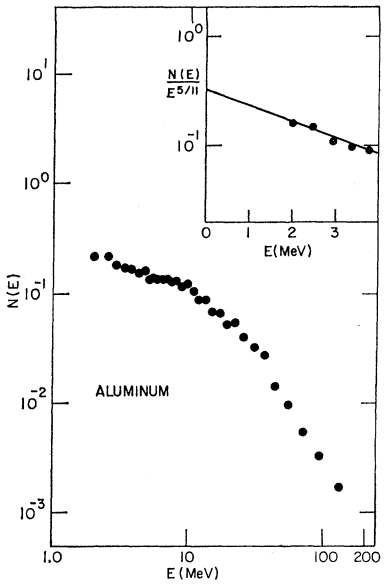

FIG. 14. Log-log plot of the neutron energy spectrum from aluminum. The inset shows a semilog plot of the low-energy part of the energy spectrum divided by $E^{5/11}$.

a preponderance of low-energy neutrons and a high-energy tail extending to ~150 MeV. Although there is no clear line of demarcation between them we distinguish two groups of neutrons. We refer to the low-energy neutrons as "evaporation" neutrons, while the remainder are referred to as the "direct" neutrons. This description follows from the view[20–23] that the capture of stopped π^- mesons in complex nuclei is a two step process. First, the π^- is captured by a pair of nucleons, either a proton-neutron pair or, less frequently,[6] a proton-proton pair. The two nucleons share the pion's rest energy and initiate nuclear cascades in which one or more nucleons (usually neutrons) may be ejected (direct emission). The energy not carried away by the direct emission is distributed among the remaining nucleons, raising the residual nucleus to a high temperature from which it deexcites by evaporating particles, mostly neutrons.

An increasing body of experimental evidence supports this general view for high-energy nuclear interactions involving complex nuclei. Where the nuclear reaction is brought about by a high-energy bombarding particle the high-energy "direct emission" appears in the forward direction while low-energy "evaporation" neutrons are emitted isotropically and dominate the backward emission. The behavior alluded to here was shown very clearly in a study by Rosen[24] of the neutron emission from nuclei bombarded with 14-MeV neutrons.

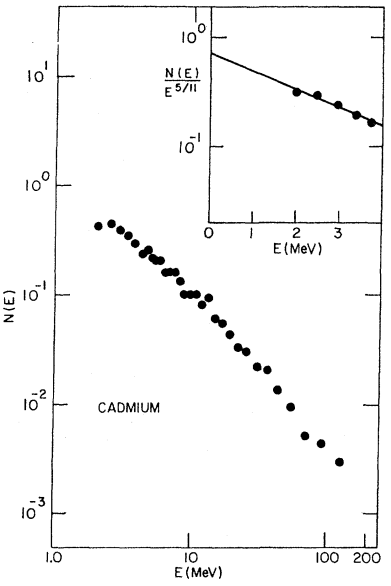

FIG. 15. Log-log plot of the neutron energy spectrum from cadmium. The inset shows a semilog plot of the low-energy part of the energy spectrum divided by $E^{5/11}$.

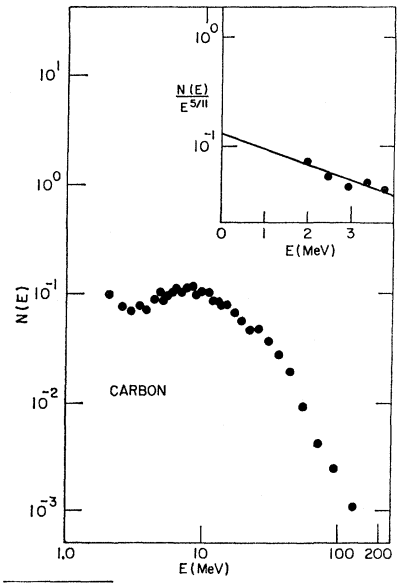

FIG. 13. Log-log plot of the neutron energy spectrum from carbon. The inset shows a semilog plot of the low-energy part of the energy spectrum divided by $E^{5/11}$.

According to Weisskopf[25] the evaporation from a nucleus in a given state of excitation could be expected to follow a Maxwellian distribution law (with temperature appropriate to the density of levels in the nucleus remaining after emission). In an evaporation cascade in which several neutrons are emitted in series, the nucleus may be cooled appreciably with the emission of each neutron. The over-all spectrum can then be expected to deviate from the simple Maxwellian form. LeCouteur[26] has shown that the resultant energy should be given approximately by

$$N_e(E)dE = KE^{5/11}\exp(-E/\theta)dE, \qquad (10)$$

[20] R. Serber, Phys. Rev. **72**, 1114 (1947).
[21] J. Heidmann and L. Leprince-Ringuet, Compt. Rend. **226**, 1716 (1948).
[22] S. Tamor, Phys. Rev. **77**, 412 (1950).
[23] P. Cuer, Compt. Rend. **231**, 846 (1950).
[24] L. Rosen, *Peaceful Uses of Atomic Energy* (United Nations, New York, 1956), Vol. 4. K. J. LeCouteur has written a review of this subject in *Nuclear Reactions*, edited by P. M. Endt and M. Demeur (North-Holland Publishing Company, Amsterdam, 1959).
[25] V. Weisskopf, Phys. Rev. **52**, 295 (1937).
[26] K. J. LeCouteur, Proc. Phys. Soc. (London) **A65**, 718 (1952).

with θ a parameter usually identified with nuclear "temperature." Accordingly, we have plotted our experimental values of $N(E)/E^{5/11}$ from 1.78 to 4.02 MeV on a semilog scale in Figs. 13 through 17. While the data in this energy region appear to follow an exponential law the fit is over a small energy region and should not be considered a verification of Eq. (10).

We fitted by least squares the initial part of the data (from 1.78 to 4.02 MeV) to a relation of the form of Eq. (10) and the parameters obtained are given in Table IV. Using Eq. (10) and the parameters K and θ obtained from the least-squares fitting we can make a rough estimate of the evaporation neutrons above 4.02 MeV by numerical integration. The remaining neutrons were classified as the "direct" neutrons. This procedure is quite uncertain, however, because it depends strongly upon the validity of the $E^{5/11}$ law, and the experiments of Gross[27] have indicated that this law may not be very reliable at high levels of excitation except for heavy nuclei (uranium). Gross used 190-MeV protons and looked for neutron emission in the backward direction. These results[27] indicate that the neutron energy spectra

TABLE IV. Summary of neutron multiplicities and kinetic energy of neutrons emitted.

Target	K	θ (MeV)	ν[a] (1.78 to 152 MeV)	ν_d	E_t (MeV)
C	0.130	3.1	2.8±0.3	2.4	68
Al	0.327	2.9	3.2±0.3	2.2	74
Cd	0.709	2.7	3.6±0.4	1.8	80
Pb	1.63	1.7	3.5±0.4	1.9	69
U	1.96	2.0	5.0±0.5	2.2	100

[a] Uncertainties include uncertainty in counter efficiency.

from medium- and low-A nuclei may be expected to give more neutrons than expected from the $E^{5/11}$ law in the region below 2 MeV. A similar conclusion is inferred from our results since extrapolating down to zero energy using the $E^{5/11}$ law and the parameters in Table IV gives neutron multiplicities which are lower than those obtained by other experimenters.[5,28,29]

It is possible to estimate the total kinetic energy (E_t) carried away by the neutrons. Most of the kinetic energy is carried away by the "direct" neutrons and the value of E_t is quite insensitive to the extrapolation below the threshold. In fact, the principal contributions to E_t come from the region where the estimate of the neutron detection efficiency is most reliable. Thus, the values obtained for this quantity, which are given in the last column of Table IV, are least subject to the uncertainties in the reduction of the data.

[27] E. E. Gross, USAEC Reports, UCRL 3330 and 3337, 1956 (unpublished). See also M. A. Preston, *Physics of the Nucleus* (Addison-Wesley Publishing Company, Inc., 1962), Chap. 17.
[28] L. Winsberg, Phys. Rev. **95**, 198 (1954).
[29] I. J. Russell, Ph.D. thesis, University of Chicago, 1956 (unpublished).

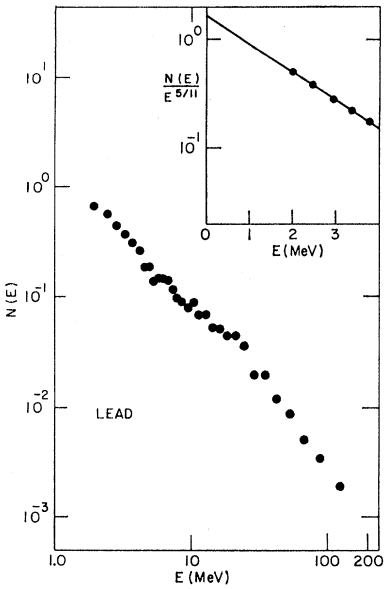

FIG. 16. Log-log plot of the neutron energy spectrum from lead. The inset shows a semilog plot of the low-energy part of the energy spectrum divided by $E^{5/11}$.

VII. DISCUSSION

The "direct" neutron spectrum has a rather similar behavior for all the targets studied. This is reflected in a fairly constant value $\nu_d \approx 2$ for the number of "direct" neutrons, and $E_t \approx 75$ MeV for the total neutron kinetic energy release. The value of E_t for uranium is somewhat higher than the other values. This is because the uranium energy spectrum shows slightly more neutrons at higher energies than the other spectra, but the effect is smaller than the uncertainty introduced in subtracting the prompt gamma-ray peak. The value of $\nu_d \approx 2$ may be considered in agreement with the value obtained by Puppi *et al.*[30,31] ($\nu_d = 1.75$ for $A = 100$).

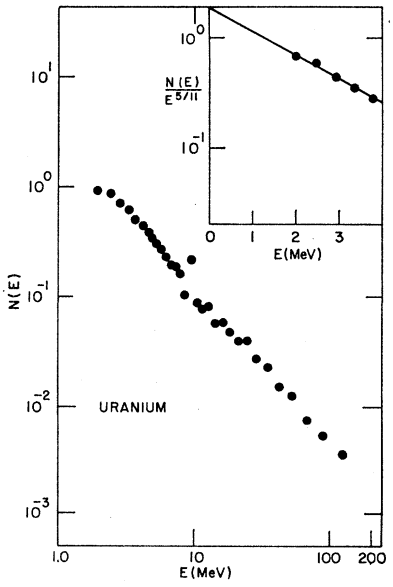

FIG. 17. Log-log plot of the neutron energy spectrum from uranium. The inset shows a semilog plot of the low-energy part of the energy spectrum divided by $E^{5/11}$.

[30] G. Puppi, V. de Sabbata, and E. Manaresi, Nuovo Cimento **9**, 726 (1952).
[31] V. de Sabatta, E. Manaresi, and G. Puppi, Nuovo Cimento **10**, 1704 (1953).

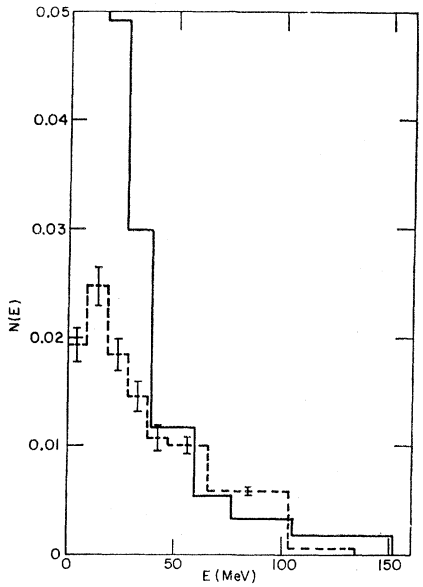

FIG. 18. Number of neutrons from Al per unit energy per π^- capture plotted against energy (solid histogram). The dashed histogram gives the results of Monte Carlo calculations (Ref. 33).

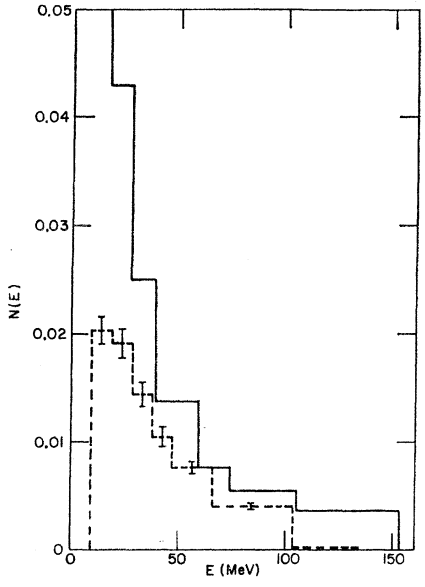

FIG. 20. Number of neutrons from U per unit energy per π^- capture plotted against energy (solid histogram). The dashed histogram gives the results of Monte Carlo calculations (Ref. 33).

We were unable to obtain meaningful values for the total neutron yields (ν_t) because of our lack of knowledge of the spectra below 1.78 MeV. In view of Gross'[27] results, uranium might be expected to follow the $E^{5/11}$ law fairly well. However, extrapolation below 1.78 MeV using the parameters in Table IV gives a multiplicity of about 7 neutrons while one expects from radiochemical studies[29] a value of 12 ± 2. The uranium multiplicity value depends, however, most strongly of all the targets on the uncertain low-energy extrapolation.

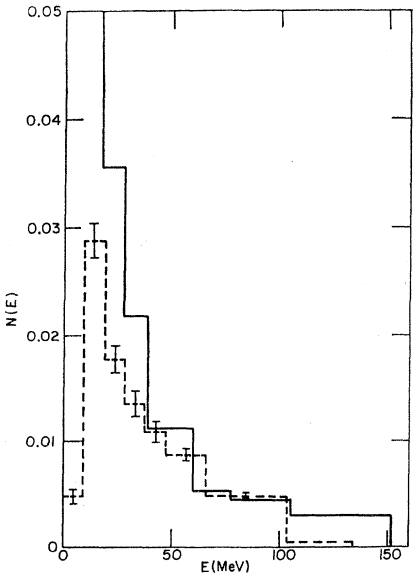

FIG. 19. Number of neutrons from Cd per unit energy per π^- capture plotted against energy (solid histogram). The dashed histogram gives the results of Monte Carlo calculations for $_{44}Ru^{100}$ (Ref. 33).

It is useful to test our results by checking the energy balance in the reaction. This is done most reliably for Cd, where charged particle emission is relatively unlikely and where we can determine the neutron multiplicity from other results. The neutron multiplicity has been measured for I^{127} ($\nu_t=6.2$) by Winsberg.[28] We adopt the value $\nu_t=6.0$ for Cd in the following estimates. The energy balance equation is

$$M_\pi-B_\pi=B(X)-B(Y)+M_n-M_p+E_{t,n}+E_{t,p}+E_{t,\gamma}, \quad (11)$$

where M_π, M_n, M_p are masses of π^-, neutron, proton, $B(X)$, $B(Y)$ are total binding energies of initial and final nuclei, X and Y, $E_{t,n}$, $E_{t,p}$ are the total kinetic energies in neutron and proton emission, $E_{t,\gamma}$ is the total γ-ray energy. B_π is the binding energy of the pion in the atomic state from which it is captured. All quantities are known except $E_{t,p}+E_{t,\gamma}=137$ MeV$-B(X)+B(Y)-E_{t,n}$. $B(X)-B(Y)$ should be a suitable average, but we will assume that $X=_{48}Cd^{113}$, and (a) $Y=_{47}Ag^{107}$ (6 neutron emission) or (b) $Y=_{46}Pd^{106}$ ($6n+1p$ emission). From Everling, *et al.*,[32] we find: $B(_{48}Cd^{113})=963.34$ MeV, $B(_{47}Ag^{107})=915.36$ MeV and $B(_{46}Pd^{106})=909.72$ MeV. Thus, we find for case (a) $E_{t,\gamma}=137-963+915-80=9$ MeV, and for case (b) $E_{t,p}+E_{t,\gamma}=137-963+910-80=4$ MeV. These values are not unreasonable, when allowance is made for uncertainties of a few MeV.

Monte Carlo calculations have been made[33] of the neutron energy spectra following low-energy π^- capture by three nuclei: $_{13}Al^{27}$, $_{44}Ru^{100}$, and $_{92}U^{238}$. In making

[32] F. Everling, L. A. König, J. H. E. Mattauch, and A. H. Wapstra, Nucl. Phys. 18, 529 (1960).
[33] A. Turkevich (private communication).

these calculations, it was assumed[34] that the π^- was captured at a random position within the nucleus by a proton-proton pair and a neutron-proton pair with equal probability. The latter assumption has been shown experimentally to be invalid.[6] In the earlier work of Puppi *et al.*,[30,31] this effect was taken into account and more captures were assumed on neutron-proton pairs than proton-proton pairs. Our results are shown plotted with the Monte Carlo results[33] as histograms in Figs. 18 through 20. Our data (from Table III) are combined into energy intervals corresponding approximately to those of the Monte Carlo calculations. In Fig. 19, we have plotted our $_{48}Cd^{112}$ results with the Monte Carlo results for $_{44}Ru^{100}$. The experimental results include the evaporation as well as the "direct" neutrons while the Monte Carlo give only the "direct" neutrons. The evaporation process is, however, negligible above 20 MeV and the spectra can be compared above this energy. The general agreement is good considering the simplicity of the model used in the calculations.

[34] N. Metropolis, R. Bivins, M. Storm, J. M. Miller, G. Friedlander, and A. Turkevich, Phys. Rev. **110**, 204 (1958).

ACKNOWLEDGMENTS

We wish to express our thanks to Professor A. Turkevich for several very helpful discussions and for making available to us previously unpublished results. In addition we would like to thank Professor N. Sugarman for very valuable advice and discussions, and Dr. A. E. Litherland for sending us details of the Owen neutron-gamma discrimination method. We would also like to thank R. Gabriel and W. Stanula for their help in the construction of equipment and in the performance of the experiment.

PHYSICAL REVIEW VOLUME 133, NUMBER 2B 27 JANUARY 1964

Neutron Transfer in $N^{14}(N^{14},N^{13})N^{15}$ at Low Energies*

G. BREIT, K. W. CHUN, AND H. G. WAHSWEILER
Yale University, New Haven, Connecticut
(Received 29 August 1963)

Formulas concerned with approximate quantum-mechanical corrections to the semiclassical (SC) treatment of the neutron transfer reaction previously contained or implied in the literature are extended and put in a more convenient form for application. New data of McIntyre, Jobes, and Becker in the laboratory energy range 9.0 to 18.0 MeV are compared with theoretical expectation. The accuracy of a previous discussion of 18-MeV data by one of the authors is improved. At 18 and at 12.6 MeV reasonable agreement with experimental angular distributions is found close to 90° in the c.m. system. At smaller angles the experimental values of the cross section are below those calculated at 18 MeV, in agreement with the influence of absorption on the recoils suggested for this case by McIntyre and Jobes; at 12.3 MeV the experimental values are somewhat smaller than the theoretical as would be the case in the presence of virtual Coulomb excitation (VCE). Total transfer cross sections show a systematic increase over expectation by a factor of about 2.9 between 9.0 and 12.8 MeV as though some VCE were present. The calculated ratio of the 90° cross section at 18 MeV to that at 12.6 MeV is about 10 times that observed. Possible explanations of this discrepancy are discussed.

I. INTRODUCTION AND NOTATION

THE neutron tunneling mechanism with special reference to the $N^{14}(N^{14},N^{13})N^{15}$ reaction has been discussed by Breit and Ebel,[1] Ebel,[2] Breit and Ebel,[3] and Breit[4] from related viewpoints. Although the quantum mechanical description of the phenomenon was already used in some of the early formulations such as,[1–3] the formulas in these papers that are useful in direct practical applications are mostly those obtained in the semiclassical (SC) approximation. The magnitude of the corrections for the quantum-mechanical character of the motion of the heavy particles has been estimated employing a δ-function potential as a representation of the effect of one of the nuclei,[4] making use of Ter-Martirosyan's evaluation[5] of an integral occurring in the theory of (n,d) reactions in terms of the hypergeometric function which is very similar to the integral obtained by Biedenharn, Boyer, and Goldstein[6] at about the same time. A treatment of the neutron

* Work supported by the U. S. Atomic Energy Commission and by the U. S. Air Force Office of Scientific Research.

[1] G. Breit and M. E. Ebel, Phys. Rev. **103**, 679 (1956). The abbreviation BE-I for this reference is occasionally used.

[2] M. E. Ebel, Phys. Rev. **103**, 958 (1956).

[3] G. Breit and M. E. Ebel, Phys. Rev. **104**, 1030 (1956). The abbreviation BE-II for this reference is occasionally used.

[4] G. Breit, *Handbuch der Physik* edited by S. Flügge (Springer-Verlag, Berlin, 1959), **41.1**, especially Sec. 48.

[5] K. A. Ter-Martirosyan, Zh. Eksperim. i Teor. Fiz. **29**, 713 (1955) [translation: Soviet Phys.—JETP **2**, 620 (1956)].

[6] L. C. Biedenharn, K. Boyer, and M. Goldstein, Phys. Rev. **104**, 383 (1956).